Simulation of quantum many-body systems by path-integral methods

E. L. Pollock and D. M. Ceperley
Lawrence Livermore National Laboratory, Livermore, California 94550
(Received 2 April 1984)

Computational techniques allowing path-integral calculations of quantum many-body systems are introduced and applied to liquid and solid helium. The computations presented in this paper do not include exchange effects. The range and limitations of the method are demonstrated by presenting thermodynamic properties, radial distribution functions, and, for the solid phase, the single-particle distribution and intermediate scattering function for imaginary times.

I. INTRODUCTION

All static properties of a many-body system in thermal equilibrium are obtainable from the density matrix

$$\rho(R,R';\beta)=\sum_s e^{-\beta E_s}\Psi_s(R)\Psi_s^*(R')\ , \tag{1.1}$$

a sum over the energy eigenstates of the system Hamiltonian, weighted by the Gibbs factor. R refers to the $3N$ particle coordinates. As seen by direct substitution the density matrix satisfies the identity

$$\rho(R,R';\beta)=\int \rho(R,R'';\beta-\beta')\rho(R'',R';\beta')dR''\ , \tag{1.2}$$

which may be iterated an arbitrary number of times (here $M-1$) to give

$$\rho(R,R';\beta)=\int\cdots\int \rho(R,R_1;\tau)\rho(R_1,R_2;\tau)\cdots \times\rho(R_{M-1},R';\tau)dR_1\cdots dR_{M-1}\ , \tag{1.3}$$

where $\tau\equiv\beta/M$. Equation (1.3) has been proposed many times as the basis for computation of the density matrix (see Ref. 1 for a partial list of references) since each density matrix in the integral corresponds to the system at a high temperature (here, $1/\tau$). At sufficiently high temperature, accurate approximations are known for the density matrix, and so the calculation reduces to a multidimensional integral, amenable, presumably, to standard Monte Carlo techniques. Computations based on Eq. (1.3) and a high-temperature approximation for the density matrix have been performed, primarily, for low-dimensional models (e.g., one-dimensional harmonic oscillator, particles in square wells). Although encouraging and instructive, these computations leave unanswered the question of the practicality of this approach for many-body systems.

In this paper a computational algorithm based, partly, on Eq. (1.3) is developed and applied to the Lennard-Jones system, with parameters appropriate to ^{4}He ($\epsilon/\kappa=10.22$ K, $\sigma_{LJ}=2.556$ Å, and $\Lambda\equiv\hbar^2/m\epsilon\sigma_{LJ}^2=0.1816$), whose high-temperature, classical,[2,3] and ground-state properties[4] have been extensively studied by other methods. Although more accurate pair potentials for helium are known, we are primarily interested in developing the methodology for a typical interaction, not in comparing with experiment. In Sec. II we introduce a Monte Carlo method for efficiently evaluating integrals with the structure of Eq. (1.3).

The density matrix can be formally symmetrized (antisymmetrized) for Bose (Fermi) statistics by summing over permutations (P),

$$\rho_P(R,R';\beta)=\frac{1}{N!}\sum_P(\pm1)^P\rho(R,PR';\beta)\ , \tag{1.4}$$

where $(\pm1)^P$ is $+1$ for bosons and the signature of the permutation for fermions. This procedure projects out eigenstates of the appropriate symmetry in Eq. (1.1). The method introduced in Sec. II does allow permutations to be sampled, which would be impossible without using some variant of the method presented there, although in this paper we do not use this feature. Fermion calculations based directly on Eq. (1.4) are not practical due to the almost complete cancellation between positive and negative terms at low temperature. Results of applying the method to fluid and solid phases are shown in Sec. III. The convergence of various averages as τ is reduced is of primary interest. The chief conclusion discussed in Sec. IV is that the method presented is capable of calculating static properties for the Lennard-Jones system studied, ignoring exchange effects, over the entire temperature range from the ground state to the classical regime. Furthermore, the computational demands on present computers are probably less than the demands made by the first molecular-dynamics studies of this system on the then available hardware. In Appendix A we review the calculation of the pair density matrix, an essential ingredient in these calculations, and tabulate some values of it. In Appendix B we give an alternative derivation for some formulas of Sec. III, and in Appendix C we derive and discuss kinetic-energy estimators.

II. COMPUTATIONAL ALGORITHM

A. High-temperature density matrix

In order to use the convolution equation (1.3) it is first necessary to find an accurate approximation to the high-temperature density matrices appearing in the integral. For this we assume a pair-product form,[1]

$$\rho(R,R';\tau)=\left[\prod_{i=1}^{N}\rho_1(r_i,r_i';\tau)\right]\left[\prod_{\substack{i,j=1\\ i<j}}^{N}\tilde{\rho}_2(r_{ij},r_{ij}';\tau)\right] . \tag{2.1}$$

Here, N is the number of atoms, $\vec{r}$ is the atomic position, and ρ_1 is the single-particle ideal-gas density matrix,

$$\rho_1(r_i,r_i';\tau)=\frac{1}{(2\pi\Lambda\tau)^{3/2}}\exp\left[-\frac{(r_i-r_i')^2}{2\Lambda\tau}\right] , \tag{2.2}$$

and $\tilde{\rho}_2$ is the two-body density matrix divided by the ideal-gas terms. For a system with a pairwise additive potential the classical limit of the density matrix, of course, is of this form. Further justification comes from the Wigner-Kirkwood corrections to this classical limit[5] where the term of order τ^2 is also of the pairwise form. Three-body terms first enter at order τ^3. At small pair separations the Wigner-Kirkwood expansion will converge only at high temperatures due to the rapid increase of the Lennard-Jones potential. Stated differently, for any temperature the pair-product approximation, Eq. (2.1), will break down for a triplet of particles having all three pair distances less than some distance r_Q which decreases as τ decreases.[6] The approximation represented by Eq. (2.1) becomes sufficiently accurate at high temperature once r_Q becomes sufficiently small that such configurations are extremely improbable.

For convenience we also make the further "end-point" approximation,

$$\tilde{\rho}(r,r';\tau)=\exp\{-\tfrac{1}{2}[P(r;\tau)+P(r';\tau)]\} , \tag{2.3}$$

for the high-temperature pair term since the one-body factors ensure that $|r-r'|\sim(\Lambda\tau)^{1/2}$ and therefore only the near-diagonal region is actually needed. Calculation of the pair density matrix is discussed in Appendix A where a tabulation of $P(r;\tau)$ for several values of τ is presented. The approximation in Eq. (2.3) also becomes exact in the limit of $\tau\to 0$, but the use of $P(r;\tau)$ rather than its high-temperature (classical) limiting form $\tau V(r)$ gives much quicker convergence with τ for any strongly interacting system. The dependence of the accuracy of the pair-product approximation, Eq. (2.1), on the particular configurations (R and R') is reflected in the slower convergence of the radial distribution function $g(r)$ at small r where the effect of small three-particle clusters can be important. Our final test for the validity of this approximation is empirical: the convergence of various expectation values as τ is decreased.

B. Metropolis Monte Carlo method

When Eq. (2.1) is substituted into Eq. (1.3) we have a multidimensional integral to evaluate. The structure of this integrand resembles that of a system of classical polymers: the discretized paths of the individual particles in what becomes a path integral as $\tau\to 0$. When Eq. (2.3) is used, the intrapolymer interaction corresponds to "spring bonds" and the interpolymer interaction is through $P(r;\tau)$. Note that for the diagonal case of primary interest, $R=R'$, these are either ring or cross-linked polymers if other than the identity permutation in Eq. (1.4) is sampled. For present purposes this polymer analogy is merely a useful intuitive way of visualizing the structure of the integrand; the analogy has been pursued further elsewhere.[7] Once the high-temperature density matrix is specified it might be expected that the remaining multidimensional integral could be evaluated by the usual Monte Carlo methods. As discussed in detail below, this method is not practical without extensive modification due to the structure of the integrand.

The Metropolis Monte Carlo procedure for sampling from any distribution—in the present case, the normalized density matrix—consists in generating a Markov process such that the desired distribution is stationary under this process.[8] Let Π_s represent the probability distribution for some state s [state in the present context refers to some configuration of the coordinates in Eq. (1.3)]. Then, by definition, the desired Markov process has transition probabilities $P_{s\to s'}$ satisfying

$$\sum_s \Pi_s P_{s\to s'}=\Pi_{s'} . \tag{2.4}$$

The common choice, due to Metropolis *et al.* (Ref. 8) is

$$P_{s\to s'}=P^*_{s\to s'}\min\left[1,\frac{\Pi_{s'}P^*_{s'\to s}}{\Pi_s P^*_{s\to s'}}\right] , \tag{2.5}$$

where P^* is an arbitrary *a priori* transition matrix and the second factor is an acceptance probability. Typically, for classical condensed-matter systems where the probability distribution to be sampled is the Gibbs distribution, the *a priori* transition consists in giving a randomly selected particle a displacement sampled from a uniform distribution.

For the integrand of Eq. (1.3) this choice of *a priori* transition matrix would be very inefficient for at least two reasons. The first reason has to do with the polymerlike nature of the integrand. The intrapolymer interaction, which becomes stronger at high temperature, and the interaction between polymers, prevent sizeable displacements of a single particle's coordinates. Moving one "bead" of a polymer is very inefficient since the rest of the polymer will, with high probability, pull it back into place on the succeeding move. In fact, for polymers it is known that the relaxation rate is approximately proportional to the polymer length squared,[9] and thus configuration space would be sampled very slowly. What is needed is a way of generating collective displacements of a large segment of "polymer" which will be accepted by the Metropolis algorithm, Eq. (2.5). A second difficulty is the impossibility of generating the permutation moves needed to simulate Bose systems, Eq. (1.4), without simultaneously altering many of the "polymer" positions. This is because each term in Eq. (1.3) corresponds to a temperature of $1/\tau$ which must be sufficiently high that Eq. (2.1) or (2.3) is an accurate approximation. This temperature is usually orders of magnitude above the lambda transition

temperature for the system (roughly the temperature where the thermal de Broglie wavelength equals the interparticle spacing, and thus exchanges are common). Consequently, generating an acceptable permutation move also entails altering many coordinates. The method we now describe largely overcomes the first difficulty and partially overcomes the second. Acceptable permutation moves can be generated with this method, but this is still rather time consuming; these boson calculations are in progress.

C. Generating *a priori* transitions

It is seen from Eq. (2.5) that with the choice $P^*_{s\to s'}=\Pi_{s'}$ the acceptance probability is one. This choice would be optimal, but is, of course, not feasible since any realistic Π_s [corresponding in our case to the normalized integrand of Eq. (1.3)] will be too complicated to sample directly. We therefore will try to approximate it as closely as possible by a form that can be directly sampled—namely a Gaussian. For this purpose the integrand of Eq. (1.3) is rewritten as

$$\rho(R,R';\beta)\left[\frac{\rho(R,R_1;\tau)\rho(R_1,R';\beta-\tau)}{\rho(R,R';\beta)}\right]\left[\frac{\rho(R_1,R_2;\tau)\rho(R_2,R';\beta-2\tau)}{\rho(R_1,R';\beta-\tau)}\right]\times\cdots$$
$$\cdots\times\left[\frac{\rho(R_{M-2},R_{M-1};\tau)\rho(R_{M-1},R';\tau)}{\rho(R_{M-2},R';2\tau)}\right], \tag{2.6}$$

noting that the added terms cancel. The terms in large parentheses are conditional probabilities for picking the next point based on the present point and the final point, R'. They are correctly normalized as is seen from Eq. (1.2). The single-particle, or ideal-gas, terms in these expressions are already Gaussians which combine to give the usual conditional probabilities[10] for a Brownian-motion path constrained to end at R'. To arrive at a useful approximation the remaining terms are expanded about the present point and the result exponentiated. To lowest order these interaction terms modify the means of the Gaussians. For example, after some algebra, the first term in large parentheses becomes

$$\frac{\rho(R,R_1;\tau)\rho(R_1,R';\beta-\tau)}{\rho(R,R';\beta)}=\left[\frac{1}{2\pi\sigma^2}\right]^{3N/2}\times\exp\left[-\frac{(R_1-R_1^*)}{2\sigma^2}\right]^2+O(\tau), \tag{2.7}$$

where

$$R_1^*=\frac{(\beta-\tau)R+\tau R'}{\beta}+\left[\frac{\beta-\tau}{\beta}\right]\tau S\,,$$

$$S(R,R';\beta)=\Lambda\nabla\ln\tilde{\rho}(R,R';\beta)\,,$$

$$\sigma^2=\tau\Lambda\left[\frac{\beta-\tau}{\beta}\right],$$

and $\tilde{\rho}$ again indicates that the free-particle part has been factored out. Similar expressions hold for the other conditional probabilities. An alternative derivation of these results is given in Appendix B. In Eq. (2.7) all interaction effects are contained in S, referred to as the velocity field, which prevents particle overlap when the next point is sampled. As written, calculating the velocity field requires the (unknown) exact density matrix for the times β, $\beta-\tau$, $\beta-2\tau$, etc. To proceed we approximate the velocity field by using a trial density matrix whose choice is discussed below.

In the actual implementation of this procedure the paths for all particles are not simultaneously altered as such a large move would very rarely be accepted by the Metropolis algorithm. Instead, all or part of the path of a selected particle is altered between fixed end points. In summary, our algorithm consists in snipping out a section of the path and then threading in a new section with the same end points using the drifting random-walk procedure of Eq. (2.7). This new path is then accepted or rejected according to Eq. (2.5). When this is extended to bosons at least two paths must be snipped and allowed to change end points. Such a procedure moves through configuration space much more rapidly than a procedure altering only a single point on the existing path. For the fluid-phase simulations discussed in Sec. III, new paths of 20 steps with $\tau=0.05$ had an acceptance ratio of about 50% for both $T^*=0.5$ and 0.2. When τ was doubled to 0.1, the acceptance ratio for 20 step modifications fell to about 20%. Of course, the choice of *a priori* transition matrix affects only the efficiency, not the final averages. The only systematic error in the calculation is the approximation in Eq. (2.1) which can be improved and checked by decreasing τ. The results of this are discussed in Sec. III after first describing the particular choice of velocity field used in the calculation.

D. Choice of velocity field

The choice of a trial density matrix used in calculating the velocity field in Eq. (2.7) is presented here. No claim for optimality is made since other choices give almost as high an acceptance ratio. In principle, it should be possible to improve any initial choice by modifying it to increase the acceptance ratio of Eq. (2.5). However, setting the velocity field to zero reduces the acceptance ratio by more than half when one particle's path is altered, and almost completely eliminates the two- and three-particle path-alteration moves needed if permutations are included.

Prandharipande and Bethe presented a method for calculating Jastrow factors in approximate ground-state wave functions for quantum fluids.[11] We use a generatization to calculate trial density matrices of the form of Eq. (2.3). When a pair-product form for the density matrix is inserted into the Bloch equation, three-body correlations are generated, which in an iterative procedure would lead to higher-body correlations.[12] To stay within a pair-product form, the three-body term can be replaced by a constant effective field chosen so that the correlation factor is unity beyond some "healing length." Specifically, we solve the equation

$$\frac{\partial f}{\partial \beta}(r;\beta)=\frac{\hbar^2}{2m}\nabla^2 f(r;\beta)-\tfrac{1}{2}[V(r)-\lambda]f(r;\beta)\ , \quad (2.8)$$

with the conditions

$$f(r;0)=1,\ \ f(r;\beta)=1\ \ (r\geq d),\ \ \frac{\partial f}{\partial r}(d;\beta)=0$$

which determines λ. The healing length d is arbitrarily taken as twice the particle-sphere radius: $d=2r_0$, $r_0=(3/4\pi\rho)^{1/3}$. The result is rather insensitive to small changes about this value. Then the velocity field is determined from

$$S=\Lambda\nabla \ln f\ , \quad (2.9)$$

or explicitly inserting particle indices,

$$S_i=\Lambda\sum_{j\ (\neq i)}\nabla_i \ln f(r_{ij};t)\ , \quad (2.10)$$

where $t=\beta, \beta-\tau$, etc. Equation (2.8) was solved numerically by the Crank-Nicholson method.

Experience using other forms for the velocity field suggests that the only feature which affects the acceptance ratio is short-range repulsion. We stress again that the choice of velocity field does not alter the final results. The final distribution of configurations is determined solely by the high-temperature density matrix, the calculation of which is reviewed in Appendix A.

III. SIMULATION RESULTS

A. Fluid phase

The convergence of this algorithm as τ is reduced has been examined at the temperatures $T^*=5.0$, 0.5, and 0.2 for the fluid density $\rho\sigma^3=0.365$. This is the experimental equilibrium density at low temperatures; ground-state computations are available for comparison.[4] In all of the fluid-phase calculations the number of particles in the periodic cell was 64. The finite-system-size effects are small and should be roughly the same as for the ground state.

The highest temperature investigated, $T^*=5.0$ ($\beta=0.2$), is over 20 times the lambda temperature for this system, so quantum effects might be expected to be small. Computations were done with $\tau=0.2$, 0.1, 0.05, 0.025, and 0.0125 corresponding to paths of 1, 2, 4, 8, and 16 steps. The results for the radial distribution function $g(r)$ listed in Table I show rapid convergence except possibly at small r. Figure 1 compares the $g(r)$ for $\tau=0.0125$ with

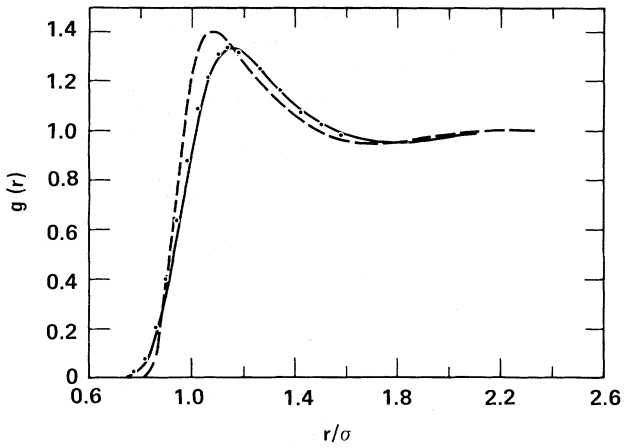

FIG. 1. Comparison of radial distribution functions $g(r)$ for Lennard-Jones system at $kT/\epsilon=5.0$, $\rho\sigma^3=0.365$, and $\Lambda=0.1816$. The most accurate results for the quantum system, using $\tau=0.0125$, are indicated by the solid line; the classical system values are indicated by the dashed line. The dots are for $\tau=0.2$, which is equivalent to a classical system with a pair potential taken from the two-particle density matrix.

that for the classical system and that from the $\tau=0.2$ calculation, which is equivalent to a classical system with the Lennard-Jones potential replaced by an effective potential obtained from the two-particle density matrix. Even at this temperature the quantum effects in $g(r)$ are seen to be significant. Use of the effective potential yields a major improvement, although errors persist inside the first peak in $g(r)$. Convergence of the kinetic-energy values given in Table II is less rapid and extrapolation to $\tau\rightarrow 0$ is necessary.

For the temperature $T^*=0.5$ ($\beta=2.0$), still over twice the lambda temperature, computations with $\tau=0.2$, 0.1, 0.05, and 0.025 corresponding to paths of 10, 20, 40, and 80 steps were done. The $g(r)$'s are listed in Table III. Convergence is slowest at small r, presumably due to the already mentioned neglect of three-body effects in the high-temperature density matrix. At this temperature use of the effective potential from the two-body solution (i.e., $\tau=2.0$) is not an accurate approximation,[13] as is seen in Fig. 2. The $g(r)$ for the classical system has a first peak height greater than 5.0 at this density and temperature.

At the lowest temperature, $T^*=0.2$, computations with $\tau=0.1$ and 0.05 corresponding to paths of 50 and 100 steps were performed. The $g(r)$ values listed in Table IV again show their slowest convergence at small r. Experimentally, the effect of Bose statistics (ignored here) is to increase the height of the first peak in $g(r)$ by about 2% for temperatures just above the lambda temperature.[14] Below this temperature $g(r)$ rapidly settles to its ground-state value, so it is relevant to compare our results to the ground-state computations of Whitlock *et al.*[4] in Fig. 3. As expected from this comparison the potential energy computed here is in good agreement with the ground-state potential energy (Ref. 4, Table V).

TABLE I. Convergence of $g(r)$ at $kT/\epsilon=5.0$ and $\rho\sigma^3=0.365$ as the number of steps (β/τ) in the path integral is increased. The numbers in parentheses indicate the uncertainty in the last digit.

r/σ	$\tau=0.2$	$\tau=0.1$	$\tau=0.5$	$\tau=0.025$	$\tau=0.0125$
0.70	3.5×10^{-4}	1.24×10^{-4}	6.9×10^{-5}	6.3×10^{-5}	1.21×10^{-4}
0.74	0.0032	0.0014	0.0012	0.0014	0.0021
0.78	0.0215	0.0118	0.0101	0.0123	0.0148
0.82	0.0791	0.0539	0.0498	0.0557	0.0611
0.86	0.2061	0.160	0.152	0.161	0.168
0.90	0.400	0.345	0.334	0.340	0.347
0.94	0.636	0.592	0.573	0.570	0.578
0.98	0.880	0.843	0.819	0.814	0.822
1.02	1.090	1.060	1.035	1.030	1.037
1.06	1.219	1.213	1.193	1.190	1.194
1.10	1.311	1.298	1.288	1.286	1.289
1.14	1.333	1.325(2)	1.331(4)	1.329(7)	1.329(8)
1.18	1.318	1.329	1.332	1.327	1.327
1.22	1.296	1.301	1.308	1.299	1.299
1.26	1.250	1.266	1.267	1.258	1.258
1.30	1.211	1.222	1.221	1.213	1.212
1.34	1.166	1.173	1.176	1.168	1.166
1.38	1.114	1.135	1.131	1.127	1.125
1.42	1.075	1.093	1.092	1.090	1.086
1.46	1.049	1.060	1.059	1.057	1.052
1.50	1.027	1.031	1.033	1.031	1.023
1.54	0.997	1.009	1.007	1.007	0.999
1.58	0.984	0.987	0.986	0.989	0.980
1.62	0.968	0.973	0.973	0.973	0.963
1.66	0.963	0.961	0.960	0.962	0.953
1.70	0.951	0.953	0.952	0.954	0.945
1.74	0.949	0.947	0.947	0.949(8)	0.940
1.78	0.949	0.946	0.944(3)	0.949	0.939(3)
1.82	0.951	0.948(8)	0.947	0.950	0.942
1.86	0.954	0.952	0.950	0.955	0.947
1.90	0.958	0.956	0.956	0.960	0.954
1.94	0.965	0.963	0.963	0.966	0.962
1.98	0.975	0.972	0.970	0.972	0.972
2.02	0.982	0.979	0.977	0.979	0.981
2.06	0.989	0.984	0.987	0.986	0.989
2.10	0.992	0.992	0.992	0.992	0.997
2.14	1.000	0.998	0.997	0.998	1.003
2.18	1.004	1.002	1.002	1.001	1.007
2.22	1.003	1.006	1.005	1.004	1.010
2.26	1.007	1.007	1.007	1.005	1.011
2.30	1.009	1.009	1.009	1.006	1.011
2.34	1.008	1.009	1.008	1.006	1.010
2.38	1.003	1.009	1.008	1.005	1.008
2.42	1.005	1.006	1.006	1.003	1.005
2.46	1.004	1.007	1.005	1.002	1.003
2.50	0.999	1.004	1.001	1.000	1.001
2.54	1.001	1.001	0.999	0.998	0.998
2.58	0.998	0.999	0.996	0.996	0.997
2.62	0.996	0.997	0.995	0.995	0.995
2.66	0.998	0.994	0.994	0.994	0.995
2.70	0.993	0.994	0.994	0.993	0.995
2.74	0.994	0.992	0.993	0.994	0.994
2.78	0.994	0.991	0.992	0.994	0.994

Our kinetic-energy estimates, extrapolated to $\tau=0$, are $\langle K\rangle/N\epsilon=1.76\pm0.05$ at $T^*=0.5$, and $\langle K\rangle/N\epsilon=1.50\pm0.05$ at $T^*=0.2$. The ground-state estimate from Ref. 4 is $\langle K\rangle/N\epsilon=1.33\pm0.01$ at this density. This is in good agreement with a linear extrapolation of our $T^*=0.5$ and 0.2 values to zero temperature.

The radial distribution functions for a classical system when the Lennard-Jones potential is replaced by a poten-

TABLE II. Convergence of potential and kinetic-energy estimates with τ. In the solid phase ($\rho\sigma^3=0.589$) some moments of the spherically density about a lattice site are given.

$\rho\sigma^3$	kT/ϵ	$\tau\epsilon$	$\langle U/N\epsilon\rangle$	$\langle K/N\epsilon\rangle$	$\langle r^2\rangle$	$\langle r^4\rangle$	$\langle r^6\rangle$
0.365	5.0	0.1	−1.648(6)	8.51(1)			
	5.0	0.05	−1.680(3)	8.33(1)			
	5.0	0.025	−1.643(3)	8.27(2)			
	5.0	0.0125	−1.604(4)	8.22(2)			
0.365	0.5	0.2	−2.081(5)				
	0.5	0.1	−2.068(2)	1.88(2)			
	0.5	0.05	−2.045(1)	1.84(2)			
	0.5	0.025	−2.025(2)	1.77(5)			
0.365	0.2	0.1	−2.053(2)	1.61(1)			
	0.2	0.05	−2.035(2)	1.56(5)			
0.589	0.2	0.1	−3.644(4)		0.093(1)	0.0147(4)	0.0033(1)
	0.4	0.1	−3.635(2)		0.094(1)	0.0151(4)	0.0035(2)

tial taken from the two-body density matrix have already been shown in Figs. 1 and 2 for $T^*=5.0$ and 0.5. At high temperature or low density this procedure would reproduce the exact quantum-mechanical result. To further study this many-body effect we now define $U(r,T,\rho)$ as that classical potential which would yield (for example, via simulation) the calculated quantum $g(r,T,\rho)$. This effective potential can be calculated by the same methods used to invert experimentally determined structure factors to obtain a molecular interaction. We used a combination of additional Monte Carlo calculations with a trial effective potential and perturbation hypernetted-chain calculations [which calculate the change in $U(r)$ needed to produce a given change in $g(r)$]. This is exactly the procedure described in Ref. 15. After two iterations we find an effective potential which produces the $g(r)$ to within the statistical error ($\sim 1\%$). The solution, however, contains considerable noise. Slowly varying functions can be added to $U(r)$, leaving $g(r)$ almost unchanged. The effective potentials (times β) are shown in Fig. 4 at $\rho\sigma^3=0.365$ and $T^*=5.0$, 1.0, 0.5, and 0.2. At high temperature ($T>5$), $U(r)$ becomes proportional to $P(r)$ (see Fig. 1 and discussion). The difference between the $\beta U(r)$ at $T^*=5.0$ plotted in Fig. 4 and the two-body values given in Appendix A is indicative of the difficulty of inverting $g(r)$ data to obtain an effective potential. Both potentials have similar structure and give quite similar $g(r)$'s, but they clearly differ by a slowly varying function of r. At low temperature we expect $\beta U(r)$ to be a zero-temperature Jastrow pseudopotential. The effective potential at zero temperature has already been calculated by Reatto,[15] whose results are similar to ours. At all temperatures the effective potential has a pronounced minimum which moves to larger r at lower temperatures, remaining always about 0.2σ beyond the maximum in $g(r)$. In addition, at lower temperatures there is a small maximum in $U(r)$ near the minimum in $g(r)$. Reatto has interpreted this as being due to roton excitations, but since our results are for Maxwell-Boltzmann rather than Bose statistics, there must be a more general explanation.

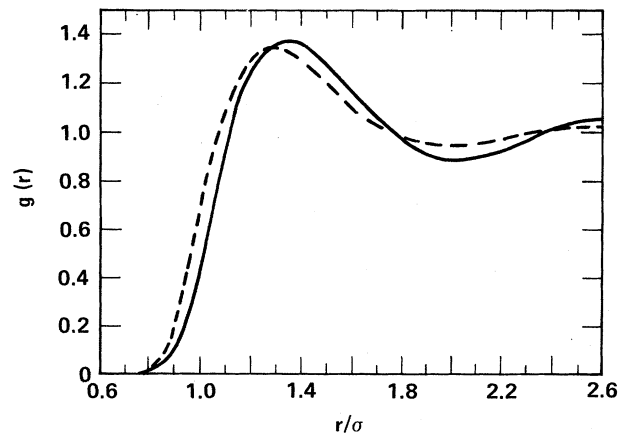

FIG. 2. Radial distribution functions at $kT/\epsilon=0.5$, $\rho\sigma^3=0.356$, and $\Lambda=0.1816$. Results from discretized–path-integral computation of 80 steps ($\tau=0.025$) (solid line) are compared with those obtained with $\tau=2.0$, one step (dashed line), equivalent to a classical system with the Lennard-Jones potential replaced by an effective potential obtained from the two-particle density matrix.

B. Solid phase

The path-integral algorithm presented here was also applied in the solid phase at $\rho\sigma^3=0.589$, where ground-state calculations have been done. Exchange effects are unimportant for the properties we calculate. These computations were for an fcc crystal of 108 particles, rather than the experimentally found hcp phase, since ground-state calculations have shown the difference in the thermodynamic properties to be less than the statistical resolution.[16] The structure factors calculated here at $T^*=0.2$

TABLE III. Same as Table I but for $kT/\epsilon=0.5$.

r/σ	$\tau=0.2$	$\tau=0.1$	$\tau=0.05$	$\tau=0.025$
0.70	2.5×10^{-5}	1.4×10^{-5}	1.2×10^{-5}	3.3×10^{-5}
0.74	3.7×10^{-4}	2.2×10^{-4}	2.2×10^{-4}	4.58×10^{-4}
0.78	0.00206	0.00186	0.00230	0.0033
0.82	0.009 69(5)	0.0105	0.0126	0.016
0.86	0.0369	0.0378	0.0435	0.0504
0.90	0.0925(7)	0.0993	0.1094	0.1181
0.94	0.193	0.204	0.215	0.225
0.98	0.339	0.348	0.357	0.366
1.02	0.511	0.522	0.521	0.529
1.06	0.695	0.696	0.694	0.703
1.10	0.879	0.864	0.862	0.869
1.14	1.038	1.013	1.011	1.018
1.18	1.165	1.137	1.140	1.145
1.22	1.251	1.237	1.241	1.243
1.26	1.311	1.307	1.311	1.310
1.30	1.341	1.350	1.355	1.352
1.34	1.361(5)	1.365(5)	1.374(5)	1.369(7)
1.38	1.356	1.367	1.371	1.363
1.42	1.332	1.347	1.353	1.344
1.46	1.307	1.320	1.319	1.311
1.50	1.265	1.277	1.280	1.270
1.54	1.224	1.230	1.232	1.223
1.58	1.178	1.184	1.183	1.175
1.62	1.130	1.135	1.134	1.126
1.66	1.086	1.087	1.086	1.080
1.70	1.042	1.043	1.042	1.038
1.74	1.004	1.004	1.002	0.999
1.78	0.970	0.969	0.967	0.966
1.82	0.944	0.941	0.938	0.938
1.86	0.922	0.916	0.915	0.915
1.90	0.904	0.899	0.898	0.900
1.94	0.894	0.888	0.886	0.888
1.98	0.886	0.881	0.880	0.882
2.02	0.886	0.881	0.880	0.883
2.06	0.887	0.885	0.884	0.888
2.10	0.897	0.895	0.893	0.896
2.14	0.906	0.905	0.904	0.907
2.18	0.921	0.920	0.919	0.921
2.22	0.934	0.935	0.935	0.937
2.26	0.951	0.952	0.953	0.954
2.30	0.968	0.968	0.970	0.972
2.34	0.985	0.985	0.985	0.988
2.38	0.999	0.999	1.001	1.003
2.42	1.010	1.013	1.014	1.017
2.46	1.019	1.026	1.024	1.027
2.50	1.023	1.034	1.033	1.035
2.54	1.030	1.040	1.039	1.040
2.58	1.036	1.042	1.043	1.044
2.62	1.043	1.044	1.043	1.044
2.66	1.040	1.044	1.043	1.044
2.70	1.035	1.043	1.040	1.041
2.74	1.032	1.036	1.036	1.036
2.78	1.031	1.032	1.031	1.031

and 0.4, using $\tau=0.1$, are given in Table V and agree with the ground-state result[4] to within the statistical error. The single-particle density $\rho(r)$ about a lattice site is compared with the published ground-state result in Fig. 5. The reason for the discrepancy at small r is unclear but amounts to less than 1% of the integrated norm due to the volume factor. The crystal is localized differently in the two calculations. It has not been possible in ground-state calculations to satisfactorily localize the particles into a solid phase using a pair-product wave function

TABLE IV. Same as Table I but for $kT/\epsilon=0.2$.

r/σ	$\tau=0.1$	$\tau=0.05$	r/σ	$\tau=0.1$	$\tau=0.05$
0.70	1.7×10^{-6}	1.1×10^{-5}	1.78	1.000	0.9985
0.74	1.5×10^{-4}	2.4×10^{-4}	1.82	0.964	0.964
0.78	0.0019	0.0022	1.86	0.939	0.937
0.82	0.00972	0.0121	1.90	0.914	0.914
0.86	0.0349	0.0412	1.94	0.898	0.896
0.90	0.0910	0.103	1.98	0.884	0.884
0.94	0.187	0.202	2.02	0.874	0.876
0.98	0.325	0.334	2.06	0.874	0.876
1.02	0.485	0.488	2.10	0.878	0.879
1.06	0.654	0.650	2.14	0.885	0.885
1.10	0.813	0.809	2.18	0.896	0.897
1.14	0.962	0.956	2.22	0.910	0.912
1.18	1.088	1.086	2.26	0.927	0.926
1.22	1.188	1.188	2.30	0.942	0.943
1.26	1.268	1.268	2.34	0.962	0.961
1.30	1.313	1.322	2.38	0.977	0.977
1.34	1.348	1.348	2.42	0.994	0.993
1.38	1.356	1.359	2.46	1.009	1.009
1.42	1.347	1.349	2.50	1.021	1.021
1.46	1.332	1.329	2.54	1.032	1.031
1.50	1.298	1.296	2.58	1.037	1.039
1.54	1.261	1.257	2.62	1.047	1.047
1.58	1.213	1.217	2.66	1.049	1.050
1.62	1.170	1.171	2.70	1.050	1.051
1.66	1.127	1.122	2.74	1.051	1.051
1.70	1.080	1.079	2.78	1.049	1.048
1.74	1.036	1.036			

alone. Additional single-particle factors—generally Gaussians about the lattice sites—are also included. A trial wave function of this latter type was used as input to the ground-state computations[4] and defines the lattice sites. In the path-integral calculations reported here the high-temperature density matrix is translationally invariant. No information about the lattice sites is input other than the initial configuration. At lower density, e.g., $\rho\sigma^3=0.365$, the system rapidly melts from this starting lattice configuration, as it should. The center of mass wanders during the course of the calculation exactly as in Monte Carlo studies on classical solids. For calculating $\rho(r)$ we keep the center of mass fixed by occasionally shifting the particles uniformly.

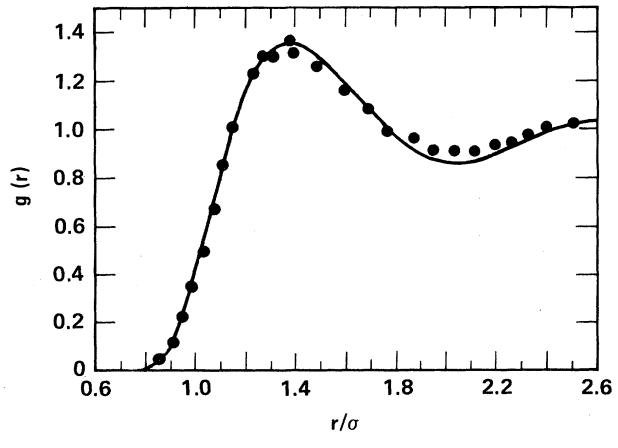

FIG. 3. Comparison of $g(r)$ for the ground-state system (●) (Ref. 4, Appendix D) with the $kT/\epsilon=0.2$, $\rho\sigma^3=0.365$ result (solid line) calculated with a path integral of 100 steps ($\tau=0.05$).

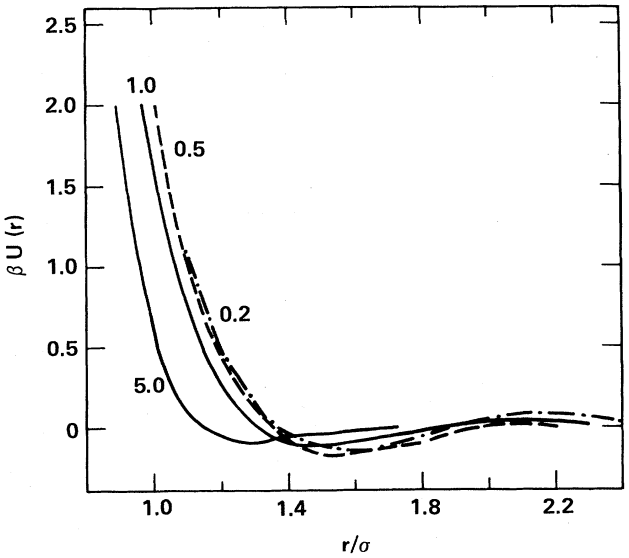

FIG. 4. Effective potentials needed in a classical system to reproduce the quantum-mechanical $g(r)$ at $\rho\sigma^3=0.365$ and indicated temperatures T^*.

TABLE V. Structure factors in fcc solid phase at $\rho\sigma^3=0.589$ for $kT/\epsilon=0.2$ and 0.4. The wave vectors are in units of $k_u=2\pi(\rho/N)^{1/3}=1.106\sigma^{-1}$.

k/k_u	$S(k)$ $(T^*=0.2)$	$S(k)$ $(T^*=0.4)$
100	0.0485(6)	0.0469(6)
110	0.0584(6)	0.0590
111	0.0689	0.0699
200	0.0924	0.0910(5)
210	0.105	0.106
211	0.118	0.116
220	0.163	0.158
221	0.172	0.170
222	0.214	0.222
300	0.158	0.161(2)
310	0.187	0.188
311	0.212	0.211
320	0.278	0.279
321	0.302	0.307
322	0.419	0.419
330	0.439	0.442
331	0.495	0.497
332	0.808	0.804
400	0.307	0.299(5)
410	0.373	0.375
411	0.423	0.431
420	0.539	0.522
421	0.600	0.598
422	0.868	0.876
430	0.651	0.655
500	0.699	0.677(18)

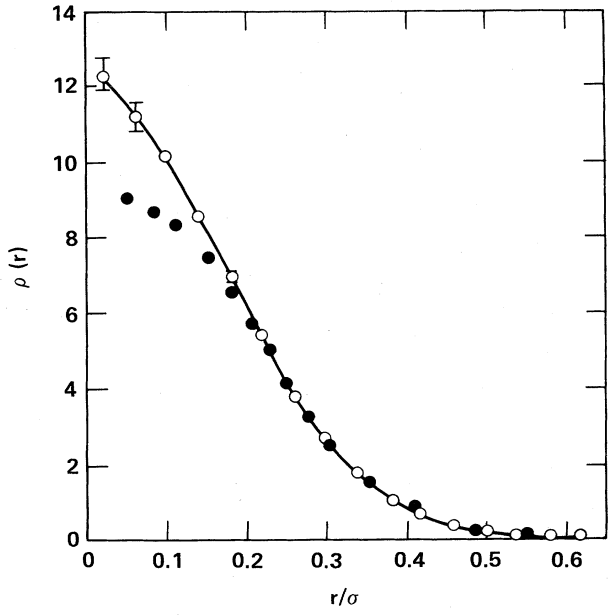

FIG. 5. Ground-state sphericalized density $\rho(r)$ about lattice site (●) and path-integral result (○) at $kT/\epsilon=0.2$ using 50 steps ($\tau=0.1$). Both computations are for an fcc lattice at $\rho\sigma^3=0.589$. The result at $kT/\epsilon=0.4$ is almost identical to the $kT/\epsilon=0.2$ result (see Table II).

C. Time correlation functions

It is straightforward to calculate imaginary-time correlation functions with the path-integral algorithm. In principle, these can be analytically continued to give the real-time correlation functions of experimental interest. This will be illustrated, along with its limitations, using the intermediate scattering function in the solid as an example.

In general, for some dynamical variable A, the time-dependent autocorrelation function is defined as

$$C(t)=\langle A(t)A(0)\rangle=\frac{1}{z}\mathrm{Tr}(e^{-\beta H}e^{iHt/\hbar}A\,e^{-iHt/\hbar}A)$$
$$=\frac{1}{z}\sum_s\sum_{s'}e^{-\beta E_s}e^{it(E_s-E_{s'})/\hbar}|\langle s|A|s'\rangle|^2$$
$$=\int_{-\infty}^{\infty}e^{-i\omega t}J(\omega)d\omega\,, \tag{3.1}$$

where $z=\mathrm{Tr}\,e^{-\beta H}$, and the spectral density

$$J(\omega)=\frac{1}{z}\sum_s\sum_{s'}e^{-\beta E_s}\delta(\omega+(E_s-E_{s'})/\hbar)|\langle s|A|s'\rangle|^2 \tag{3.2}$$

has the property

$$J(-\omega)=e^{-\beta\omega}J(\omega)\,. \tag{3.3}$$

For imaginary times $\Upsilon=it/\hbar$ the relations become

$$C(\Upsilon)=\frac{1}{z}\mathrm{Tr}(e^{-H(\beta-\Upsilon)}A\,e^{-H\Upsilon}A)$$
$$=\frac{1}{z}\mathrm{Tr}[\rho(\beta-\Upsilon)A\rho(\Upsilon)A],\quad 0\le\Upsilon\le\beta \tag{3.4}$$

which is easily calculated in the path-integral algorithm, if A is a function of the system coordinates, by averaging the value of A at any point along the path multiplied by its value at the point Υ/τ steps further along the path. The symmetry $C(\Upsilon)=C(\beta-\Upsilon)$ is evident from Eq. (3.4). The problem is now to continue $C(\Upsilon)$ from imaginary to real times, or, equivalently, to invert

$$C(\Upsilon)=\int_{-\infty}^{\infty}e^{-\omega\Upsilon}J(\omega)d\omega$$
$$=\int_0^{\infty}J(\omega)(e^{-\omega\Upsilon}+e^{-\omega(\beta-\Upsilon)})d\omega \tag{3.5}$$

for the spectral density $J(\omega)$. In addition to the computed $C(\Upsilon)$, a few of the initial time derivatives

$$C^{(n)}(t=0)=\int_{-\infty}^{\infty}(-i\omega)^nJ(\omega)d\omega$$
$$=(i/\hbar)^n\langle[H,\cdots[H,[H,A]]\cdots]A\rangle \tag{3.6}$$

(n factors of H) may be known.

This is equivalent to the problem of analytically continuing the thermal Green's function,[17] and a formal inversion of Eq. (3.5) can be obtained. Writing

$$C(\Upsilon)=\sum_{n=-\infty}^{\infty}e^{-iZ_n\Upsilon}\Gamma_n,\quad Z_n=2\pi n/\beta \tag{3.7}$$

satisfies the condition $C(0)=C(\beta)$ where the Fourier coefficients

$$\Gamma_n=\frac{1}{\beta}\int_0^\beta e^{iZ_n\Upsilon}C(\Upsilon)d\Upsilon$$
$$=\frac{1}{\beta}\int_{-\infty}^{\infty}\frac{e^{-\beta\omega}-1}{iZ_n-\omega}J(\omega)d\omega$$
$$=\frac{2}{\beta}\int_0^\infty\frac{e^{-\beta\omega}-1}{(iZ_n)^2-\omega^2}\omega J(\omega)d\omega\ , \tag{3.8}$$

using Eq. (3.5). Defining the function

$$\Gamma(Z)=\frac{1}{\beta}\int_{-\infty}^{\infty}\frac{e^{-\beta\omega}-1}{Z-\omega}J(\omega)$$
$$=\frac{2}{\beta}\int_0^\infty\frac{e^{-\beta\omega}-1}{Z^2-\omega^2}\omega J(\omega)d\omega\ , \tag{3.9}$$

the asymptotic behavior of which is related to the initial time derivatives

$$\Gamma(Z)\to\frac{2}{\beta}\frac{\langle[H,A]A\rangle}{Z^2}+O(1/Z^4)\ , \tag{3.10}$$

gives an inversion formula[17]

$$J(\omega)=\frac{\beta}{2\pi i}\frac{1}{e^{-\beta\omega}-1}$$
$$\times\lim_{\epsilon\to0+}[\Gamma(Z=\omega-i\epsilon)-\Gamma(Z=\omega+i\epsilon)]\ . \tag{3.11}$$

The function $\Gamma(Z)=\Gamma_n$ when $Z=iZ_n$ and it is the unique analytic function also satisfying the asymptotic condition (3.11).

To use this inversion formula on numerical data, an analytic function with the correct asymptotic property and satisfying $\Gamma(Z)=\Gamma_n$ at as many $Z=iZ_n$ as possible must be constructed.[18] A Padé approximant in Z^2, where the numerator is a polynomial of degree $N-1$ and the denominator is of degree N, can satisfy the asymptotic behavior, Eq. (3.10), which reduces the number of unknown coefficients by one. If more initial time derivatives are known, the number of coefficients to be determined is further reduced. The remaining $2N-1$ coefficients are determined by equating the Padé approximant to Γ_n at $Z=iz_n$ for $n=0,1,\ldots,2N-2$. The resulting spectral density function obtained from Eq. (3.11) consists of $2N$ δ functions at $\omega=\pm\omega_j$ where the ω_j^2 $(j=1,\ldots,N)$ are the poles of the Padé approximant.

This formalism is of very limited use in the present computations. To determine more than one or two poles requires a precision in $C(\Upsilon)$ not possible in Monte Carlo computations. By way of illustration the intermediate scattering function

$$F(k,\Upsilon)=\frac{1}{N}\langle\rho_k(\Upsilon)\rho_{-k}(0)\rangle,\quad \rho_k=\sum_{j=1}^{N}e^{ik\cdot r_j} \tag{3.12}$$

was calculated in the solid phase. The value at the origin, $F(k,0)=S(k)$, and the initial time derivative,

$$\frac{dF(k,0)}{d(\Upsilon\epsilon)}=-\frac{\Lambda}{2}(k\sigma)^2$$

(in reduced units), determines a single δ-function approximation to $J(\omega)$ corresponding physically to an excitation with no damping. In Fig. 6 this approximation is seen to match the computed $C(\Upsilon)$ almost within the error bars. It is possible to use the method presented above to determine a few additional δ functions, but these give no further insight into the actual $J(\omega)$ or any indication, for example, of excitation lifetimes.

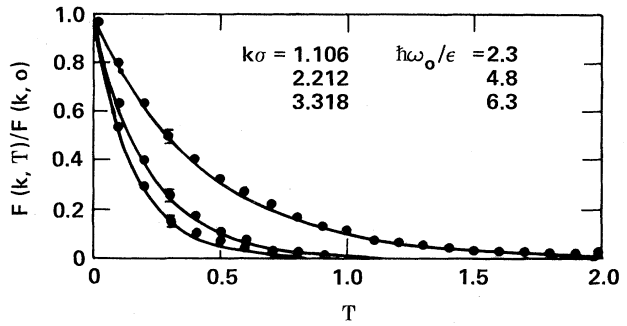

FIG. 6. Imaginary-time intermediate scattering funtion, Eq. (3.12), in the fcc solid phase at $\rho\sigma^3=0.589$ and $kT/\epsilon=0.2$. The solid lines are the undamped phonon approximation, the frequencies of which are listed beside the k vectors (all in [100] direction). These frequencies give a rough estimate of the longitudinal sound velocity along [100] as 720—750 m/sec.

In Ref. 19 a method of calculating $J(\omega)$ directly, rather than by inversion of $C(\Upsilon)$ data, was suggested. Although the particular method suggested there appears very difficult to apply to this system, the idea should be pursued.

IV. CONCLUSIONS

It has been demonstrated that the path-integral method can be used to compute the static properties of quantum systems, ignoring statistics, over a wide range of conditions. For the Lennard-Jones system studied here this range extends from the classical regime to the ground-state limit. One drawback of our path-integral computations is the necessary investigation of path-discretization errors ($\tau\neq0$) which requires several computations with varying τ. In principle, this can be eliminated with the use of a Green's-function Monte Carlo procedure.[20] A more serious question is whether these methods can be extended to include Bose and Fermi statistics.

Bosons have been treated by an extension of the method presented here, although the introduction of new permutations occurs so rarely that convergence of the algorithm has not been demonstrated. More physical insight is needed into the selection of new permutations and configurations to increase the acceptance ratio and adequately sample permutation space. Treating fermions is difficult, even in ground-state calculations, and we are trying to extend some of the approximations used there to finite temperatures. It appears that path-integral computations will yield only limited information about real-time dynamics.

ACKNOWLEDGMENTS

The authors thank Dr. B. J. Alder for his interest in this work and help in revising an earlier draft of this paper. This work was performed under the auspices of the U.S. Department of Energy by the Lawrence Livermore National Laboratory under Contract No. W-7405-ENG-48.

APPENDIX A: CALCULATION OF THE PAIR DENSITY MATRIX

In the path-integral algorithm described above all input about the system is contained in the high-temperature density matrix. For systems with pair interactions the density matrix reduces to a product of pair density matrices at sufficiently high temperature. This appendix reviews three methods of calculating this essential ingredient.

The Monte Carlo method, discussed first, is not the most efficient method for a two-body problem, but is presented because it can be applied, essentially unmodified, to few-body problems where there are no alternatives, and it is the easiest of the three methods to program. The "matrix squaring method" of Klemm and Storer[21,22] is then reviewed and a tabulation of results obtained with this method is given. Finally, the eigenfunction expansion of the pair density matrix is discussed.

1. Monte Carlo method

The pair density matrix for the Lennard-Jones system can be written, in reduced units, as

$$\rho(\vec{r}_1,\vec{r}_2;\vec{r}\,'_1,\vec{r}\,'_2;\beta)=\rho_{\text{c.m.}}(\vec{R},\vec{R}';\beta)\rho_{\text{rel}}(\vec{r},\vec{r}\,';\beta)\ , \tag{A1}$$

where the center-of-mass term is

$$\rho_{\text{c.m.}}(\vec{R},\vec{R}';\beta)=\frac{e^{-(R-R')^2/\Lambda\beta}}{(\pi\Lambda\beta)^{3/2}}\ ,$$

with $R=(r_1+r_2)/2$ and $\Lambda=\hbar^2/m\epsilon\sigma_{\text{LJ}}^2$. The density matrix for the relative coordinate satisfies the equation

$$\frac{\partial\rho_{\text{rel}}}{\partial\beta}(\vec{r},\vec{r}\,';\beta)=[\Lambda\nabla^2-V(r)]\rho_{\text{rel}}(\vec{r},\vec{r}\,';\beta)\ , \tag{A2}$$

where $\vec{r}=\vec{r}_1-\vec{r}_2$, with initial condition

$$\rho_{\text{rel}}(\vec{r},\vec{r}\,';0)=\delta(\vec{r}-\vec{r}\,')\ .$$

In the following we drop the subscript "rel" and the vector arrows and introduce the function

$$f(r;t\mid r_o,r_f\beta)\equiv\rho(r,r_o;t)\rho_T(r,r_f;\beta-t)\ ,$$

where $\rho_T(r_o,r_f;\beta-t)$ is an input trial density matrix satisfying

$$\rho_T(r,r_f;0)=\delta(r-r_f)\ ,$$

and r_o and r_f are the original and final relative coordinates. From the above definition it follows that

$$\rho(r_o,r_f;\beta)=\rho_T(r_o,r_f;\beta)\frac{f(r_f;\beta\mid r_o,r_f;\beta)}{f(r_o;0\mid r_o,r_f;\beta)}\ . \tag{A3}$$

Using Eq. (A2), f satisfies the equation

$$\frac{\partial f}{\partial t}=\Lambda\nabla^2 f-\nabla\cdot(fs)+Bf\ , \tag{A4}$$

where the "velocity field" is given by

$$s(r,r_f;\beta-t)=2\Lambda\nabla\ln\rho_T(r,r_f;\beta-t)\ ,$$

and the "birth rate" is given by

$$B(r,r_f;\beta-t)=\frac{1}{\rho_T(r,r_f;\beta-t)}\times\left[\frac{\partial}{\partial t}+\Lambda\nabla^2-V(r)\right]\rho_T(r,r_f;\beta-t)\ .$$

Note that the birth rate would be zero if ρ_T were the exact density matrix. Formally, the solution to Eq. (A4) may be written, also using (A3), as

$$\rho(r_o,r_f;\beta)=\rho_T(r_o,r_f;\beta)\times\left\langle\exp\left[\int_0^\beta B(r',r_f;\beta-t')dt'\right]\right\rangle_{\text{DRW}}\ , \tag{A5}$$

where $\langle\ \rangle_{\text{DRW}}$ denotes an average over all drifting random walks, i.e., those generated by ignoring the birth-rate term in Eq. (A4). Equation (A5) is derived heuristically by considering sufficiently small time steps so that the birth rate acts independently of the diffusion and drift terms. Considering the full solution as a product of these small time steps leads to this path-integral solution. If ρ_T were taken as merely the free-particle density matrix, then Eq. (A5) would become the familiar Feynman-Kac formula,[23] which is not suitable as a computational algorithm for systems with rapidly varying potentials. A well-chosen ρ_T, in addition to guaranteeing that the paths reach r_f at "time" β, should produce a smooth birth rate.

The drifting random walks needed to evaluate Eq. (A5) can be generated from the short-time limit of the Green's function of Eq. (A4), neglecting the birth-rate term,

$$G(r_2;t_2\mid r_1;t_1,r_f;\beta)=\frac{\exp[-(r_2-r^*)^2/2\sigma^2]}{(2\pi\sigma^2)^{3/2}}\ , \tag{A6}$$

with

$$r^*=\left[\frac{\beta-t_2}{\beta-t_1}\right]\left[r_1+\frac{\tau}{\beta-t_2}r_f+\tau s\right]\ ,$$

$$s=2\Lambda\nabla\ln\tilde{\rho}_T(r_1,r_f;\beta-t_2)\ ,$$

$$\tau=t_2-t_1\ ,$$

$$\sigma^2=2\Lambda\tau\left[\frac{\beta-t_2}{\beta-t_1}\right]\ ,$$

and $\tilde{\rho}_T$ is the nonideal part of the trial density matrix.

This procedure has been used to calculate pair density matrices for the Lennard-Jones system. The trial density matrix used had the form

$$\tilde{\rho}_T(r,r_f;\beta-t)=\exp\left[\frac{P_T(r;\beta-t)+P_T(r_f;\beta-t)}{2}\right]\ ,$$

where

$$P_T(r;\beta-t)=1\Big/\left[\frac{5\sqrt{\Lambda}r^5}{4}+\frac{r^{12}}{4(\beta-t)}\right]\ ,$$

which reduces to $4(\beta-t)/r^{12}$ when $\beta-t\to 0$ (high temperatures) and to the WKB approximation to the ground-state form when $\beta-t\to\infty$. The paths were generated from (A6) using a predictor-corrector approach:[24] s is

TABLE VI. Values of the diagonal part of the two-body density matrix [$P(r;\tau)$ defined in Eq. (2.3)] calculated using the matrix squaring method of Appendix A. Beyond the r values listed the semiclassical approximation, $P(r;\tau)=\tau V(r)+(\tau^2\Lambda/12)\nabla^2 V(r)$, where $\tau=1./T^*$, is sufficiently accurate.

r/σ	$T^*=5.0$	$T^*=10.0$	$T^*=20.0$	$T^*=40.0$	$T^*=80.0$
0.650	14.19(2)	13.14(5)	11.5(1)	9.174(4)	6.375
0.675	11.41(2)	10.36	8.78	6.70	4.378
0.700	9.20	8.16	6.68	4.83	2.97
0.725	7.36	6.39	5.03	3.44	1.995
0.750	5.93	4.99	3.75	2.41	1.325
0.775	4.71	3.86	2.76	1.67	0.887
0.800	3.75	2.94	2.00	1.14	0.572
0.825	2.956(5)	2.23	1.42	0.76	0.371
0.850	2.31	1.66(1)	0.99	0.50	0.243
0.875	1.79	1.21	0.67	0.32	0.151
0.900	1.351	0.856(5)	0.44	0.20	0.0922
0.925	1.00	0.59	0.28	0.121	0.0539
0.950	0.72	0.385	0.16	0.067	0.0289
0.975	0.50	0.236	0.088	0.031	0.0129
1.000	0.326(4)	0.126(5)	0.034	0.008	0.002
1.025	0.188	0.047	0.004	−0.006	−0.0045
1.050	0.0833	−0.006	−0.022	−0.015	−0.0087
1.075	0.007	−0.0396	−0.035	−0.020	−0.0108
1.100	−0.053	−0.063	−0.042	−0.023	−0.0119
1.125	−0.089	−0.076	−0.045	−0.024	−0.0122
1.150	−0.114	−0.081	−0.046	−0.024	−0.0121
1.175	−0.131(3)	−0.084	−0.045	−0.023	−0.0116
1.200	−0.138	−0.082	−0.043	−0.022	−0.0111
1.225	−0.139	−0.079	−0.041	−0.021	−0.0104
1.250	−0.137	−0.075	−0.038	−0.019	−0.0096
1.275	−0.133	−0.071	−0.036	−0.018	−0.0089
1.300	−0.127	−0.066	−0.033	−0.0164	−0.0082
1.325	−0.119	−0.061	−0.030	−0.0151	
1.350	−0.111	−0.056	−0.028	−0.0139	
1.375	−0.1028	−0.051	−0.026	−0.0127	
1.400	−0.0944	−0.047	−0.023	−0.0116	
1.425	−0.0868	−0.043	−0.021		
1.450	−0.0803	−0.0393	−0.019		
1.475	−0.0735	−0.036	−0.018		
1.500	−0.0673	−0.0329(7)	−0.0162(6)		
1.525	−0.0617				
1.550	−0.0568				
1.575	−0.0517				
1.600	−0.0474				

calculated at r_1 and a predicted r_2 chosen where s is reevaluated. The average s is then used for the final drift step. The birth-rate integral in Eq. (A5) was evaluated by the trapezoidal rule.

In addition to the statistical uncertainties due to the finite number of paths generated, there is a systematic error due to the finite-time step τ. As in the many-body case this is estimated by repeating the calculation for various τ values (here, typically, $\tau=0.01$, 0.005, and 0.001). Since the total number of time steps is β/τ, this procedure is more time consuming at lower temperatures. Using 20 000 paths, values for the diagonal density matrix accurate to better than 10^{-3} for the temperatures of Table VI were obtained. The finite-time-step error could be eliminated by using the Green's-function Monte Carlo method,[20] which is, however, much more complicated.

2. Matrix squaring method

Originally used by Klemm and Storer and since rediscovered many times, the matrix squaring method is based on Eq. (1.2),

$$\rho(\vec{r}_1,\vec{r}_2;\beta)=\int d\vec{r}_3\rho(\vec{r}_1,r_3;\beta/2)\rho(\vec{r}_3,\vec{r}_2;\beta/2)\ , \quad \text{(A7)}$$

together with the observation that if the density matrix can be stored for all values of r_1 and r_2, then each iteration results in a factor-of-2 reduction in the starting temperature. This is only practical for low-dimensional systems. As written, Eq. (A7) is a three-dimensional integral; however, a partial-wave expansion,

$$\rho(\vec{r}_1,\vec{r}_2;\beta)=\sum_{l=0}^{\infty}\frac{2l+1}{4\pi r_1 r_2}\rho_l(r_1,r_2;\beta)P_l(\cos\theta_{12})\ ,$$

gives a one-dimensional integral for each partial wave,

$$\rho_l(\vec{r}_1,\vec{r}_2;\beta)=\int dr_3\rho_l(r_1,r_3;\beta/2)\rho_l(r_3,r_2;\beta/2)\ . \tag{A8}$$

If the integral is evaluated by the trapezoidal rule the iteration reduces to matrix squaring. The starting temperature is taken sufficiently high that the density matrices are accurately given by their semiclassical values. To correct for the truncation of the integral at the upper limit the matrix of stored values of ρ_l is surrounded by a strip within which the ρ_l are replaced by their semiclassical values scaled by the ratio of calculated to semiclassical values at the nearest inside boundary.[22] This boundary correction is necessary to obtain accurate results. At high temperatures the density matrix is increasingly diagonal. This has two effects: a sufficiently fine grid must be used so that the starting high-temperature density matrix is well approximated, and an increasing number of partial waves are required. Partial waves beyond some maximum are approximated by their semiclassical values.

With sensible values of the starting temperature, maximum number of partial waves, grid size, and integration cutoff, this method gives accurate results as verified both by internal consistency and comparison with other methods. Computationally, it is considerably less time consuming than the other two methods. The pair density matrices used in this paper were computed by this method and are given in Table VI. Forty partial waves were computed, the starting temperature was 2^8 times the final temperature, and a grid was chosen so that $(4\Lambda/T_{\max})^{1/2}>3\Delta r$.

3. Expansion in eigenfunctions

The solution to Eq. (A2) may be written as a sum over energy eigenstates weighted with the Gibbs factor. For the Λ values for helium ($\Lambda=0.1816$) the Lennard-Jones system has no bound states, and this sum is an integral over continuum states

$$\rho_{\rm rel}(\vec{r},\vec{r}\,';\beta)=\sum_{l=0}^{\infty}\frac{2l+1}{2\pi^2}\frac{P_l(\cos\theta)}{rr'}\times\int dk\, e^{-\beta\Lambda k^2}R_{kl}(r)R_{kl}(r')\ ,$$

where the radial wave functions satisfy

$$\Lambda\left[-\frac{d^2}{dr^2}+\frac{l(l+1)}{r^2}\right]R_{kl}(r)+V(r)R_{kl}(r)=\Lambda k^2R_{kl}(r)\ .$$

This method was used in the first accurate calculations of Lennard-Jones pair density matrices at low temperatures.[25] At higher temperatures it is less convenient, both because more partial waves must be calculated and higher-energy eigenstates contribute to the integral. Consequently, the same accuracy was more easily obtained with the matrix squaring method for the temperatures shown in Table VI.

For the case of the Coulomb potential where the full density matrix can be obtained from the $l=0$ term,[21] and efficient packages to calculate Coulombic wave functions are available,[26] this method is quite convenient.

APPENDIX B: DERIVATION OF DRIFTING RANDOM-WALK METHOD

This appendix contains a different derivation of the drifting random-walk method of sampling new configurations. Let the conditional probability to be sampled from Eq. (2.7) be denoted as

$$f(R;t)=\frac{\rho(R_o,R;t)\rho(R,R_f;\beta-t)}{\rho(R_o,R_f;\beta)}\ . \tag{B1}$$

Here, R_o and R_f are the original and final points of the walk. As argued in the text we expect f to be Gaussian-like for all t; hence it is characterized by a mean and variance:

$$R^*(t)=\int dR\,Rf(R;t)\ , \tag{B2}$$

$$\sigma^2_{\alpha\beta}(t)=\int dR[R-R^*(t)]_\alpha[R-R^*(t)]_\beta f(R;t)\ , \tag{B3}$$

where α and β refer to Cartesian components. $R^*(t)$ and $\sigma^2(t)$ can be developed in a power-series expansion in t about zero as we illustrate here for the first term. Taking the t derivative of Eq. (B2) and using the Bloch equation gives

$$\frac{dR^*(t)}{dt}=\frac{1}{\rho(R_o,R_f;\beta)}\times\int dR\,R[-\rho(R,R_f;\beta-t)H\rho(R_o,R;t)+\rho(R_o,R;t)H\rho(R,R_f;\beta-t)]\ , \tag{B4}$$

where H is the system Hamiltonian. Using the explicit form for H and applying Green's theorem we are left with

$$\frac{dR^*(t)}{dt}=\frac{\Lambda}{\rho(R_o,R_f;\beta)}\int dR\,\rho(R_o,R;t)\nabla\rho(R,R_f;\beta-t)\ . \tag{B5}$$

Evaluating this for $t=0$ gives

$$\frac{dR^*(t)}{dt}=\Lambda\nabla\ln\rho(R_o,R_f;\beta)\ . \tag{B6}$$

Continuing in the same manner we arrive at the exact power series:

$$R^*(t)=R_o+t\Lambda\nabla\ln\rho(R_o,R_f;\beta)+\Lambda\frac{t^2}{2}\nabla V(R_o)+O(t^3)\ ,$$
$$\sigma^2_{\alpha\beta}(t)=t\Lambda\delta_{\alpha\beta}+t^2\Lambda^2\nabla_\alpha\nabla_\beta\ln\rho(R_o,R_f;\beta)+O(t^3)\ . \tag{B7}$$

Substituting the pair-product form, Eq. (2.1), into this expression gives Eq. (2.7) to order t.

APPENDIX C: KINETIC-ENERGY ESTIMATION

In this appendix we collect formulas and remarks about estimating the kinetic energy. From Eq. (1.1) the kinetic energy can be calculated as

$$\frac{\langle K\rangle}{\epsilon}=\frac{\frac{-\Lambda}{2}\int\lim_{R\to R'}\sum_{i=1}^{N}\nabla_i^2\rho(R,R';\beta)dR}{\int\rho(R,R;\beta)dR}\ . \tag{C1}$$

If the density matrix is calculated from Eqs. (1.3) and (2.3), this becomes

$$\frac{\langle K\rangle}{N\epsilon}=\frac{3}{2\tau}-\frac{\langle (R^i-R_1^i)^2\rangle}{2\Lambda\tau^2}-\frac{\langle (R^i-R_1^i)\cdot\nabla_i P(R;\tau)\rangle}{2} +\frac{\Lambda}{4}\left[\langle\nabla_i^2 P(R;\tau)\rangle-\frac{\langle[\nabla_i P(R;\tau)]^2\rangle}{2}\right], \quad \text{(C2)}$$

where R and R_1 are separated by one step along the path. For the ideal gas ($P=0$) this estimator does not give the exact result of $3/2\beta$ for the Maxwell-Boltzmann case for every configuration, since the average squared displacement term varies. It has been noted that for solvable models such as the ideal gas or harmonic oscillator the variance of this estimator increases as the path discretization is reduced (i.e., smaller τ).[27]

An alternative estimator which does give the exact answer with zero variance for the ideal-gas case can be derived as follows. We note that the kinetic energy is obtainable from the δ^2 term in the expansion of

$$I(\delta)=\int\rho(R_1+M\delta,R_1;\beta)dR_1 =\int\rho(R_1+M\delta,R_2;\tau)\rho(R_2,R_3;\tau)\cdots \times\rho(R_M,R_1;\tau)dR_1\cdots dR_M\ , \quad \text{(C3)}$$

where the second line is from Eq. (1.3). We now make the change of variables

$$R_1=R_1,\ R_2=R_2-(M-1)\delta\ ,$$

and

$$R_3=R_3-(M-2)\delta,\ \ldots,\ R_M=R_M-\delta$$

in the integral. Expanding in δ and using the high-temperature density matrix of Eq. (2.3), the new estimator for the kinetic energy is then

$$\frac{\langle K\rangle}{N\epsilon}=\frac{3}{2\beta}+\frac{\Lambda}{2}\left[\frac{1}{3}+\frac{1}{6M^2}\right]\left\langle\sum_{K=1}^{M}\nabla_i^2 P(R_K;\tau)\right\rangle -\frac{\Lambda}{2}\left\langle\left[\sum_{K=1}^{M}C_K\nabla_i P(R_K;\tau)\right]^2\right\rangle$$

$$\text{with } C_K=\left[\frac{M+1-K}{M}\right]\left[1-\frac{\delta_{K,1}}{2}\right]. \quad \text{(C4)}$$

This estimator clearly produces the exact result in the ideal-gas case and when quantum effects are absent (i.e., $\Lambda\to 0$). Unfortunately, the variances of the old and the new estimators are roughly the same for paths of only a few steps, and for long paths the old estimator, Eq. (C2), has a much smaller variance than the new. Accordingly, the kinetic-energy values given in Table II were estimated with Eq. (C2). Equations (C2) and (C4) represent the two limits of displacing one step in the path or of spreading the displacement over the entire path, and it is possible that an estimator corresponding to some intermediate case would have a smaller variance than either of these. This was not investigated.

Finally, the pressure is equal to two-thirds the kinetic-energy density plus the usual virial term (which can be calculated from the radial distribution function).

[1] J. A. Barker, J. Chem. Phys. **70**, 2914 (1979).
[2] L. Verlet, Phys. Rev. **165**, 201 (1968).
[3] A. Rahman, Phys. Rev. **136**, 405 (1964).
[4] P. A. Whitlock, D. M. Ceperley, G. V. Chester, and M. H. Kalos, Phys. Rev. B **19**, 5598 (1979).
[5] L. D. Landau and E. M. Lifshitz, *Statistical Physics* (Pergamon, New York, 1977), Eq. (33.20).
[6] These remarks are confirmed by explicit calculation of the three-body density matrix using the Monte Carlo method described in Appendix A. The pair-product approximation becomes accurate to smaller and smaller separations as the temperature increases. The approximation overestimates the density matrix for a collinear configuration of three particles, but is an underestimate for an equilateral-triangle configuration.
[7] D. Chandler and P. G. Wolynes, J. Chem. Phys. **74**, 4078 (1981).
[8] N. Metropolis, A. W. Rosenbluth, M. N. Rosenbluth, A. H. Teller, and E. Teller, J. Chem. Phys. **21**, 1087 (1953).
[9] D. E. Rouse, J. Chem. Phys. **21**, 1272 (1953).
[10] F. B. Knight, *Essentials of Brownian Motion and Diffusion* (American Mathematical Society, Providence, R.I., 1981).
[11] V. R. Pandharipande and H. A. Bethe, Phys. Rev. C **7**, 1312 (1973).
[12] T. Dunn and A. A. Broyles, Phys. Rev. **157**, 156 (1967).
[13] L. W. Bruch, I. J. McGee, and R. D. Murphy, J. Low Temp. Phys. **35**, 185 (1979).
[14] E. C. Svenson, V. F. Sears, A. D. B. Woods, and P. Martel, Phys. Rev. B **21**, 3638 (1980).
[15] L. Reatto, in *NATO Workshop on Monte Carlo Methods in Quantum Problems,* edited by M. H. Kalos (Reidel, Dordrecht, The Netherlands, 1984), Vol. 125C.
[16] P. A. Whitlock, M. H. Kalos, G. V. Chester, and D. M. Ceperley, Phys. Rev. B **21**, 999 (1980).
[17] A. L. Fetter and J. D. Walecka, *Quantum Theory of Many-Particle Systems* (McGraw-Hill, New York, 1971), Sec. 31.
[18] D. Thirumalai and B. J. Berne, J. Chem. Phys. **79**, 5029 (1983).
[19] J. E. Hirsch and J. R. Schrieffer, Phys. Rev. B **28**, 5353, (1983).
[20] P. A. Whitlock and M. H. Kalos, J. Comput. Phys. **30**, 361 (1979).
[21] R. G. Storer, J. Math Phys. **9**, 964 (1968).
[22] A. D. Klemm and R. G. Storer, Aust. J. Phys. **26**, 43 (1973).
[23] R. P. Feynman, *Statistical Mechanics* (Benjamin, Reading, Mass., 1972).
[24] E. Helfand, Bell Syst. Tech. J. **58**, 2289 (1979).
[25] S. Y. Larsen, K. Witte, and J. E. Kilpatrick, J. Chem. Phys. **44**, 213 (1969).
[26] A. R. Barnett, J. Comput. Phys. **46**, 171 (1982). A. R. Barnett, D. H. Feng, J. W. Steed, and L. J. B. Goldfarb, Comput. Phys. Commun. **8**, 377 (1974).
[27] M. F. Herman, E. J. Bruskin, and B. J. Berne, J. Chem. Phys. **76**, 5150 (1982).